Micromechanical Mixer-Filters ("Mixlers")

Ark-Chew Wong, *Member, IEEE,* and Clark T.-C. Nguyen, *Senior Member, IEEE*

***Abstract*—A device comprised of interlinked micromechanical resonators with capacitive mixer transducers has been demonstrated to perform both frequency translation (i.e., mixing) and highly selective low-loss filtering of applied electrical input signals. In particular, successful downconversion of a 200-MHz radio frequency (RF) signal down to a 37-MHz intermediate frequency (IF) and subsequent high-Q bandpass filtering at the IF are demonstrated using this single, passive, micromechanical device, all with less than 13 dB of combined mixing conversion and filter insertion loss. The mixer-filter (or "mixler") RF-to-IF voltage transfer function is shown to depend upon a ratio of local oscillator amplitude and applied bias voltages. [796]**

***Index Terms*—Bandpass filter, electromechanical coupling, IF, intermediate frequency, microelectromechanical systems (MEMS), microelectromechanical devices, mixer, quality factor, resonator, VHF.**

I. Introduction

SUPERHETERODYNE communication receivers rely heavily on both highly selective filtering and low-loss low-noise mixing for frequency channel selection and downconversion. To maximize performance, these mixing and filtering functions are most often achieved via separate and distinct components that must interface with one another at the board level. The use of separate components for mixing and IF filtering not only places limits on the degree of size reduction possible in portable communication devices, but can also entail added power consumption if special drivers are required to properly match the output of the mixer to the subsequent filter. Furthermore, impedance mismatches between the mixer output and filter input can contribute additional insertion loss in the receive and transmit paths.

Recent advances in micromachining technologies that yield high-Q, high frequency, micromechanical ("μmechanical") resonators [1]–[3] may now offer a method for combining both of these functions into a single passive, microscale device that eliminates mixer-to-filter connection losses. This paper reports on such a device, comprised of interlinked micromechanical resonators with capacitive mixer transducers, that downconverts radio frequency (RF) signals from 200 MHz down to a 37-MHz intermediate frequency (IF), then performs high-Q filtering, all with less than 13 dB of combined mixing conversion and filter insertion loss, and with ideally zero dc power consumption [4]. With a 13-dB combined conversion-insertion loss on par with or better than that of mixer and IF filter component combinations used in today's wireless handsets [5]–[7], this device may potentially replace both the filtering and mixing functions in heterodyning wireless communication transceivers (as shown in Fig. 1), reducing both size (by orders of magnitude) and power consumption over the off-chip macroscopic counterparts often used in current systems. Since this device performs both mixing and high-Q filtering in a single micromechanical structure, it will be called a "mixer-filter" or "mixler" for the remainder of this paper.

Manuscript received January 4, 2002; revised October 5, 2003. This work was supported by the Defense Advanced Research Projects Agency (DARPA) by Grant F30602-97-2-0101. Subject Editor S. D. Senturia.

A.-C. Wong is with Globespanvirata, Irvine, CA USA.

C. T.-C. Nguygen is with DARPA/MTO, Arlington, VA 22203 USA (e-mail: cnguyen@darpa.mil).

Digital Object Identifier 10.1109/JMEMS.2003.823218

II. Mixler Structure and Operation

Fig. 1(b) presents a schematic describing the structure and operation of the micromechanical mixler device. As shown, the basic structure of this device mimics that of a μmechanical filter [8], comprised of two clamped-clamped beam μresonators, each with center frequency $f_{\rm IF}$, coupled at low-velocity locations by a flexural mode beam. As such, the device operates by first converting an electrical input signal to a mechanical force, then processing this signal mechanically via its network of flexural-mode beams, then reconverting the resulting signal to an electrical output signal that can be further processed by subsequent transceiver electronics. This structure, however, differs from previous filters in that the coupling beam is now highly resistive to reduce local oscillator-to-IF-output (LO-to-IF) coupling, and additional electrodes have been provided to increase the tunability and functionality of each μmechanical resonator. In particular, three rectangular polysilicon strips underlie each μmechanical resonator, one centered at the midpoint of the resonator beam and serving as an input/output (I/O) electrode, and the others placed symmetrically around the I/O electrode, serving as frequency tuning electrodes [9], [10]. Also, the gaps between the electrodes and resonators are now only 325 Å—in contrast to over 1000 Å in previous work—in order to maximize electromechanical couplings at the input and frequency pulling transducers. Finally, electrodes are now also placed at each resonator anchor to allow the application of voltages across a resonator for localized annealing [12], [13], which can greatly enhance the performance of a given filter under contaminated environments.

The key to mixing in this device is in its capacitive electromechanical transducer, which converts electrical energy (i.e., voltage) to mechanical energy (i.e., force) via a square law transfer function. In particular, the z-directed force exerted between the input electrode and resonator beam shown in Fig. 2 can be expressed as the derivative of the energy E stored in the electrode-to-resonator capacitor with respect to resonator beam displacement z. In terms of variables from Fig. 2, and assuming

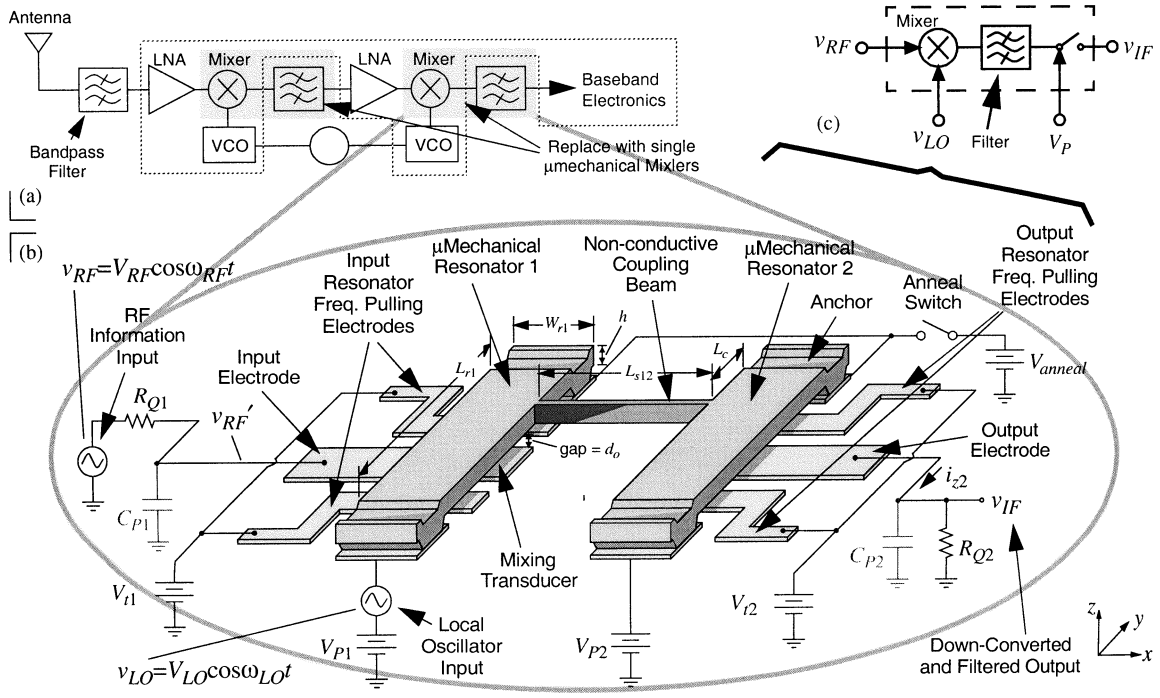

Fig. 1. (a) Simplified block diagram of a wireless receiver, indicating (with shading) the components replaceable by the subject mixler devices. (b) Schematic diagram of the described μmechanical mixler, depicting the bias and excitation scheme needed for downconversion. (c) Equivalent block diagram of the mixler scheme.

for now that the tuning electrodes $t1$ and $t2$ are given the same dc potential as the beam, this force can be expressed as

$$F_z = \frac{\partial E}{\partial z} = \frac{\partial}{\partial z}\left[\frac{1}{2}C_1(v_e - v_b)^2\right] = \frac{1}{2}(v_e^2 - 2v_b v_e + v_b^2)\frac{\partial C_1}{\partial z} \quad (1)$$

where v_e and v_b are the voltages applied to the electrode and conductive resonator beam, respectively, C_1 is the input electrode-to-resonator capacitance, which is a function of both displacement z and time t, and $(\partial C_1/\partial z)$ is the effective change in resonator-to-electrode capacitance per unit displacement, given by (2) shown at the bottom of the page, where $k_r(y)$ is the total resonator stiffness (including both mechanical and electrical components) at location y, k_{re} is $k_r(y)$ evaluated at $y = L_r/2$, $Z_{\mathrm{mode}}(y)$ is a function describing the mode shape of the beam during resonance, ε_o is the permittivity in vacuum, and geometric variables are defined in Figs. 1(b) and 2. Equation (2) differs from previous expressions [8], since it includes the effects of static beam bending and distributed stiffness by integrating these quantities over the electrode width.

Note that any of the voltage product terms in the final form of (1) is capable of mixing when presented with an appropriate set of input signals. In particular, as governed by (1), the capacitively transduced device of Fig. 2 operates as a voltage-to-force

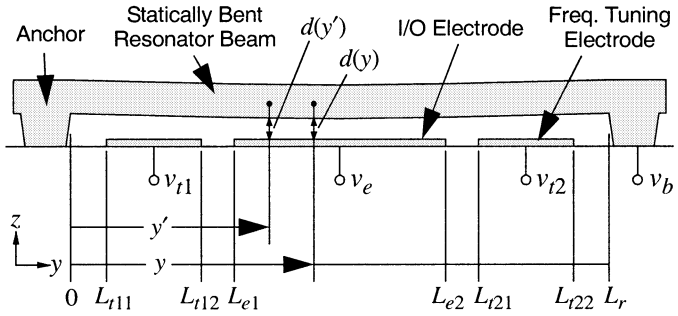

Fig. 2. Cross-sectional schematic of the idealized three-port clamped-clamped beam micromechanical end resonator used in the mixler device, identifying terminal locations, and specifying key dimensional variables used in the analytical formulations derived in the text. $d(y) = d_o$ for an unbent beam.

mixer when signals are applied to terminals e and b such that the difference voltage $(v_e - v_b)$ contains the sum or difference of the local oscillator signal v_{LO} and the RF input signal v_{RF}. In addition, as will be seen, $(v_e - v_b)$ must also contain a dc-bias voltage V_P for filter termination purposes.

One set of input placements that satisfies the above criteria is shown in Fig. 1(b), where a local oscillator input v_{LO} with frequency f_{LO} is applied to the input resonator; an information (or RF) input v_{RF} with frequency $f_{\mathrm{RF}} = f_{\mathrm{IF}} + f_{\mathrm{LO}}$ (consistent with actual inputs to communication transceivers) is applied to the R_{Q1}-terminated input electrode; and dc-bias voltages V_{P1}

$$\frac{\partial C_i}{\partial z} = \sqrt{\int_{L_{e1}}^{L_{e2}}\int_{L_{e1}}^{L_{e2}} \frac{(\varepsilon_0 W_r)^2}{[d(y')d(y)]^2}\frac{k_{re}}{k_r(y')}\frac{Z_{\mathrm{mode}}(y)}{Z_{\mathrm{mode}}(y')}dy'dy} \quad (2)$$

and V_{P2} are applied to the input and output resonators, respectively, in the filter structure. With this input configuration, the z-directed force F_z applied to the input resonator beam expands to

$$F_z = \frac{\partial E}{\partial z} = \frac{1}{2}(v_{\rm RF} - V_{P1} - v_{\rm LO})^2 \left(\frac{\partial C_1}{\partial z}\right) = \frac{1}{2}V_{P1}^2\frac{\partial C_1}{\partial z} + \frac{1}{2}v_{\rm RF}^2\frac{\partial C_1}{\partial z} + \frac{1}{2}v_{\rm LO}^2\frac{\partial C_1}{\partial z} + V_{P1}v_{\rm LO}\frac{\partial C_1}{\partial z} - V_{P1}v_{\rm RF}\frac{\partial C_1}{\partial z} - v_{\rm LO}v_{\rm RF}\frac{\partial C_1}{\partial z}. \quad (3)$$

The last term in (3) represents the mixing term of interest. In particular, in the simple case where the RF input signal $v_{\rm RF}$ and the local oscillator signal $v_{\rm LO}$ are pure sinusoids, given by $v_{\rm RF} = V_{\rm RF}\cos\omega_{\rm RF}t$ and $v_{\rm LO} = V_{\rm LO}\cos\omega_{\rm LO}t$, respectively, the last term of (3) expands to include the term

$$F_{\rm mix} = \cdots - \frac{1}{2}V_{\rm RF}V_{\rm LO}\frac{\partial C_1}{\partial z}\cos\underbrace{(\omega_{\rm RF} - \omega_{\rm LO})t}_{\omega_{\rm IF}} + \cdots \quad (4)$$

which clearly indicates a mixing of *voltage* signals $v_{\rm RF}$ and $v_{\rm LO}$ down to a *force* signal at frequency $\omega_{\rm IF} = (\omega_{\rm RF} - \omega_{\rm LO})$. If the capacitive transducer generating this force is used to couple into a μmechanical filter with a passband centered at $\omega_{\rm IF}$ as shown in Fig. 1(b), an effective mixler device results that provides both a mixer and filtering function in one passive, micromechanical device. Note that even though none of the applied signals shown in Fig. 1(b) is within the IF passband of the micromechanical filter structure, a *force* component *within* the filter passband still arises at the input due to quadratic nonlinearity in the voltage-to-force capacitive input transducer. This in-band force then drives the filter input resonator of Fig. 1(b) into vibration, generating a mechanical displacement signal z, that is then processed (i.e., filtered) mechanically by the succeeding network of beams, then reconverted to an electrical signal by the dc-biased, time varying capacitor at the output transducer. This output signal will have a frequency within the IF passband around $\omega_{\rm IF}$ and a current magnitude into the output resistor R_{Q2} given by

$$i_{z2} = V_{P2}\frac{\partial C_2}{\partial z}\frac{\partial z}{\partial t} \quad (5)$$

where dC_2/dz is the incremental change in electrode-to-resonator capacitance at the output transducer (of resonator 2).

In addition to the mixing term, (3) contains several other terms, each of which warrants closer inspection to insure that it does not introduce unwanted interference in the mixler output. Pursuant to this, the first term in (3) represents an off-resonance dc force that statically bends the beam, but that otherwise has little effect on its signal processing function, especially for very high frequency (VHF) and above applications, for which the beam stiffness is very large.

The second, third, fourth, and fifth terms represent forces capable of driving the input beam into resonance if the applied voltages are such that the frequency of the resulting force falls within the passband of the filter structure in Fig. 1(b). In particular, the second and third terms can resonate the input beam if either $v_{\rm LO}$ or $v_{\rm RF}$ contain components with frequencies near (1/2) $\omega_{\rm IF}$. The fourth and fifth terms can excite resonance if either $v_{\rm LO}$ or $v_{\rm RF}$ contain components with frequencies near $\omega_{\rm IF}$. For the present mixing application, forces generated by the second through fifth terms of (3) constitute interferers, and thus, input components at (1/2) $\omega_{\rm IF}$ and $\omega_{\rm IF}$ must be suppressed. Fortunately, in the vast majority of present-day communication architectures, mixler inputs at (1/2) $\omega_{\rm IF}$ and $\omega_{\rm IF}$ are very unlikely, since bandpass filters preceding the mixers usually remove such components.

TABLE I
MIXING INPUT CONFIGURATIONS

Description	v_e	v_b
RF I/O Input (V_P on beam)	v_{RF}	V_P+v_{LO}
RF I/O Input (V_P on I/O)	V_P+v_{RF}	$v_{\rm LO}$
RF/Carrier on I/O Input	v_{RF}+v_{LO}	$V_{\rm P}$
RF/Carrier on Beam Input	$V_{\rm P}$	v_{RF}+v_{LO}
RF Beam Input (V_P on beam)	$v_{\rm LO}$	V_P+v_{RF}
RF Beam Input (V_P on I/O)	V_P+v_{LO}	$v_{\rm RF}$
I/O Input	V_P+v_{RF}+v_{LO}	0
Beam Input	0	V_P+v_{RF}+v_{LO}

As stated earlier, the excitation configuration used in Fig. 1(b), although the most convenient for this work, is certainly not the only configuration that produces mixing. As such, Table I summarizes other possible input configurations for mixing.

III. MIXLER DESIGN

The design specification for this device encompasses both mixer and filter requirements, and thus, includes metrics for IF frequency $f_{\rm IF}$, filter bandwidth B, filter shape factor S, and overall noise figure F. The design procedure for this device derives from that for a micromechanical filter at the needed IF frequency [8], but with significant differences and additional constraints set by mixer requirements. As such, the design procedure for a mixler based on clamped-clamped beam μmechanical resonators can be itemized as follows:

1) Design a micromechanical resonator with a resonance frequency corresponding to the desired mixler IF center frequency $\omega_{\rm IF}$ and with input electrode dimensions capable of achieving a desired termination impedance R_{Q1} under mixer input biasing conditions;
2) design the filter network of the mixler, using a plurality of nonconductive coupling beams and micromechanical resonators; and
3) set the IF impedance and noise figure of the mixler via appropriate choice of dc-bias voltage V_P and local oscillator zero-to-peak amplitude $V_{\rm LO}$.

To better specify the exact design procedure, Table II presents a step-by-step summary of the design process for a μmechanical mixler device and specifies all needed equations. The specific procedure shown corresponds to the case where the desired specifications include the filter center frequency $\omega_{\rm IF}$, the bandwidth B, the termination resistor values R_{Q1} and R_{Q2}, and the local oscillator voltage amplitudes V_{LO1}

TABLE II
MICROMECHANICAL MIXLER DESIGN (USING CC-BEAMS) SUMMARY

Objective/Procedure		Relevant Design Equations for a Given Parameter
Given: f_{IF}, $R_{Q1}=R_{Q2}$, V_{LO1}, $V_{LO2}=0$V Find: L_r, V_{P1}, V_{P2} 1. Choose E, ρ, and ν by choice of structural material. 2. Choose W_r, W_e, d_o, and $h_{reff}=f(h)$. 3. Generate an expression for $d(y)$ [8]. 4. Simultaneously solve $\Im_1(L_r, V_{P2}) = R_{Q2}$ (6) $\Im_2(L_r, V_{P2}) = f_{IF}$ (7) for L_r and V_{P2}. 5. Calculate V_{P1} using $V_{P1} = \sqrt{V_{P2}^2 - 0.5V_{LO1}^2}$ (8) Note: The above design procedure assumes $V_{t11}=V_{t12}=V_{P1}$ and $V_{t21}=V_{t22}=V_{P2}$. These are to be adjusted to correct for finite fabrication tolerances.	R_{Qn}	$R_{Q1} = \left[\frac{Q}{q_1 Q_{fltr}} - 1\right] R_{z1}'$, $\Im_1(L_r, V_P) = R_{Q2} = \left[\frac{Q}{q_2 Q_{fltr}} - 1\right] R_{z2}$ (9) $R_{z1}' = \frac{k_{re}}{\omega_o Q (V_{P1}^2 + 0.5V_{LO}^2)(\partial C_1/\partial z)^2}$, $R_{z2} = \frac{k_{re}}{\omega_o Q V_{P2}^2 (\partial C_2/\partial z)^2}$ (10) $\frac{\partial C_i}{\partial z} = \sqrt{\int_{L_{e1}}^{L_{e2}} \int_{L_{e1}}^{L_{e2}} \frac{(\varepsilon_o W_r)^2}{[d(y')d(y)]^2} \frac{k_{re}}{k_r(y')} \frac{Z_{mode}(y)}{Z_{mode}(y')} dy' dy}$, $k_{re} = k_r\big\vert_{y = L_r/2}$, (11) $d(y) = d_o - \frac{1}{2} V_P^2 \varepsilon_o W_r \left(\int_{L_{e1}}^{L_{e2}} \aleph(y) dy' + \int_{L_{t11}}^{L_{t12}} \aleph(y) dy' \right)$, $\aleph(y) = \frac{1}{k_m(y')(d(y'))^2} \frac{Z_{mode}(y)}{Z_{mode}(y')}$ (12)
	f_{IF}	$\Im_2(L_r, V_P) = f_{ri} = f_{nom} \left[1 - \langle \frac{k_{ei}}{k_m} \rangle - \langle \frac{k_{eit}}{k_m} \rangle \right]^{1/2}$ (13) $\langle \frac{k_{ei}}{k_m} \rangle = \int_{L_{e1}}^{L_{e2}} \frac{(V_{Pi}^2 + 0.5V_{LOi}^2)\varepsilon_o W_r}{[d(y)]^3 k_m(y)} dy$, $\langle \frac{k_{eit}}{k_m} \rangle = 2 \int_{L_{t11}}^{L_{t12}} \frac{((V_{Pi} - V_{ti})^2 + 0.5V_{LOi}^2)\varepsilon_o W_r}{[d(y)]^3 k_m(y)} dy$ (14) $m_r(y) = \frac{\rho W_r h_{reff} \int_0^{L_r} [Z_{mode}(y')]^2 (dy')}{[Z_{mode}(y)]^2}$, $k_r(y) = \omega_o^2 m_r(y)$, $k_m(y) = [2\pi f_{nom}]^2 m_r(y)$ (15)
	f_{nom}	$\tan\frac{\beta}{2} + \frac{\beta}{\alpha}\left(\frac{\alpha^2 + g^2(\kappa G/E)}{\beta^2 - g^2(\kappa G/E)}\right)\tanh\frac{\alpha}{2} = 0$, $\left\{\frac{\alpha^2}{\beta^2}\right\} = \frac{g^2}{2}\left[\mp\left(1 + \frac{E}{\kappa G}\right) + \sqrt{\left(1 - \frac{E}{\kappa G}\right)^2 + \frac{4L_r^2 h_{reff} W_r}{g^2 I_r}}\right]$ (16) $I_r = \frac{W_r h_{reff}^3}{12}$, $G = \frac{E}{2(1+\nu)}$, $g^2 = [2\pi f_{nom}]^2 L_r^2 \left(\frac{\rho}{E}\right)$ (17)
Find: L_{s12} 1. Choose W_{s12}. 2. Solve $\Im_3 = 0$ for L_{s12}.	L_{s12}	$\Im_3(L_{s12}) = \sinh\varphi\cos\varphi + \cosh\varphi\sin\varphi$, $\varphi = L_{s12}\left[\frac{\rho W_{s12} h_{reff} \omega_{IF}^2}{E I_{s12}}\right]^{1/4}$, $I_{s12} = \frac{W_{s12} h_{reff}^3}{12}$ (18)
Given: B Find: L_c 1. Solve (19) for L_c.	L_c	$k_r(y = L_c) = \frac{f_o k_{s12}}{B k_{12}}$, $k_{s12} = -\frac{E I_{s12} \varphi^3 (\sin\varphi + \sinh\varphi)}{L_{s12}^3 (\cos\varphi\cosh\varphi - 1)}$ (19)

and V_{LO2}, and the parameters to be found that define the final design are the resonator length L_r, the applied dc-bias voltages V_{P1} and V_{P2}, the coupling beam length L_{s12}, and the coupling beam-to-resonator beam attachment location L_c.

The design procedure starts with the simultaneous solution of equations for resonance frequency and termination resistance, (9)–(17), to find the needed values for the resonator beam length L_r and the dc-bias voltage V_{P2} for the output resonator, for which $V_{LO2} = 0$ V is assumed. The needed value for V_{P1} is then determined by solving the expression

$$V_{P1}^2 + 0.5V_{LO1}^2 = V_{p2}^2 \tag{20}$$

which must hold if the input and output resonators (with identically dimensioned I/O and frequency tuning electrodes) are to have identical resonance frequencies. After obtaining values that satisfy frequency and termination requirements, coupling beam dimensions and attachment locations are then determined to satisfy quarter-wavelength and bandwidth requirements using a procedure identical to that used in conventional μmechanical filter design [8].

Several of the equations in Table II differ significantly from those used in conventional micromechanical filter design [8]. In particular, the equations associated with resonance frequency and termination impedance determination now contain dependences on the local oscillator voltage amplitude V_{LOi} and on the frequency tuning electrode dimensions. The major differences are now discussed in detail.

A. Resonance Frequency

As explained in [8], when designed with identical resonators and with quarter-wavelength coupling beams, the center frequency of a micromechanical filter $f_{\rm IF}$ is equal to the center frequency of each resonator. Thus, accurate expressions for the resonance frequency of a clamped-clamped beam micromechanical resonator *under mixer conditions* are paramount.

Mixer conditions differ from those of previous work [8] in that the beam is subjected to not only the dc-bias voltage V_P, but also to the large off-resonance ac voltage $v_{\rm LO}$, both of which influence its resonance frequency by generating electrical stiffnesses [8]–[11]. As such, the expression for the resonance frequency for a clamped-clamped beam with both I/O and frequency tuning electrodes, and under the mixer conditions of

Fig. 1(b), differs from a previous expression [8] mainly in the frequency tuning factor, and can be written as

$$f_{\rm IF} = f_{\rm nom}\left(1 - \left\langle \frac{k_{ei}}{k_m}\right\rangle - \left\langle \frac{k_{eit}}{k_m}\right\rangle\right)^{1/2} \tag{21}$$

where $f_{\rm nom}$ is the resonance frequency of an ideal clamped-clamped beam with a uniform rectangular cross section and in the absence of electromechanical coupling, and $\langle k_{ei}/k_m\rangle$ and $\langle k_{eit}/k_m\rangle$ are electrical-to-mechanical stiffness ratios integrated over the I/O and tuning electrode widths, respectively, of resonator i, and satisfying the relations (assuming $V_{LOi} \gg V_{RFi}$, and with reference to Fig. 2)

$$\left\langle \frac{k_{ei}}{k_m}\right\rangle = \int_{L_{e1}}^{L_{e2}} \frac{(V_{Pi}^2 + 0.5V_{LOi}^2)\varepsilon_0 W_r}{[d(y)]^3 k_m(y)}dy \tag{22}$$

$$\left\langle \frac{k_{eit}}{k_m}\right\rangle = 2\int_{L_{t11}}^{L_{12}} \frac{((V_P - V_{ti})^2 + 0.5V_{LOi}^2)\varepsilon_0 W_r}{[d(y)]^3 k_m(y)}dy \tag{23}$$

where ε_o is the permittivity in vacuum, $k_m(y)$ is the location-dependent *mechanical* stiffness under conditions where there is no electromechanical coupling, given by (15) [8], $V_{LOi} = 0$ V for $i = 2$, geometric and electrical variables are defined in Figs. 1(b) and 2, and where (23) assumes two, identical, symmetrically placed tuning electrodes as in Fig. 1(b).

Equations (16) and (17) in Table II comprise Timoshenko-derived formulations that can be solved for the mechanical resonance frequency $f_{\rm nom}$ of a z-directed beam in the absence of electromechanical coupling [14], [15]. Note that the Timoshenko theory used to obtain these equations includes the effects of shear displacements and rotary inertia, and so apply even for beams with small length-to-thickness ratios—a common case for VHF-range resonator applications. In addition, note that instead of the actual physical thickness h, all equations in Table II use an effective thickness $h_{\rm reff}$, to be extracted later in Section V, which accounts for the effects of topography on clamped-clamped beams. $h_{\rm reff}$ absorbs the topography correction constant of [8].

From (21)–(23), it should be clear that the frequencies of the micromechanical resonators in a mixler device can be significantly perturbed via application of the local oscillator signal $v_{\rm LO}$. As shown in Fig. 1(b), the best input configuration for a mixler with a nonconductive coupling beam is one where the local oscillator signal is applied to only the input resonator and not to the output resonator. This isolates the dc-biased output resonator from the LO signal, and thus, greatly suppresses LO feedthrough to the IF output port. In this configuration, however, (21)–(23) predict that the frequencies of the input and output resonator cannot be identical in the absence of some form of frequency compensation or tuning. Frequency compensation is best done by adjusting V_{P1} relative to V_{P2} according to (8) in the left column of Table II, which, as will be seen in Section IV, also happens to set $R_{Q1} = R_{Q2}$. If tuning electrodes are available, as in Fig. 1(b), then this can also be done while maintaining $V_{P1} = V_{P2}$ by applying appropriate voltages to the tuning electrodes to match the frequencies of each resonator. In this case, however, R_{Q1} must be different from R_{Q2}.

B. Mixler IF Termination Impedance

Although it receives inputs at frequencies far from resonance, vibrational displacements in the micromechanical filter of this mixler device still occur only at frequencies within its IF passband. Thus, any biasing or circuit strategy used to control or influence the filter's performance must be designed to generate or operate on signals at frequencies within the IF passband. In particular, the value for the termination impedances R_{Q1} and R_{Q2} for a mixler, which are needed to control the Qs of the input and output resonators so as to flatten the passband of the mechanical filter portion [8], must be determined based upon voltages, currents, and motions at IF passband frequencies. Note, however, that this does not preclude the influence of the local oscillator signal $v_{\rm LO}$, which in the end actually greatly impacts the value of R_{Qi} by generating force components at the resonance frequency.

To illustrate, we first recognize that R_{Q1} and R_{Q2} essentially provide series feedback at the input and output resonator ports, generating ac feedback voltages that oppose the associated resonator's motion when it vibrates, lowering its displacement amplitude, and thus, lowering its Q. Pursuant to obtaining a quantitative expression governing Q-control of the input resonator (i.e., resonator 1) by R_{Q1}, Fig. 3 presents a perspective-view schematic for a resistively loaded mixler I/O resonator, explicitly defining key variables, and in particular, identifying an effective point input force F_i and an effective point feedback (Q-controlling) force F_{fb}, both located at the midpoint of the beam and obtained via integration over the electrode width. Using the directions defined in this figure, the displacement z at the resonator beam midpoint resulting from a force at resonance $F_i = |F_i|\cos\omega_{\rm IF}t$ applied at this point is governed by

$$z = \frac{Q(F_i + F_{fb})}{jk_{re}} \tag{24}$$

where Q is the unloaded quality factor of the resonator beam and k_{re} is the stiffness at the midpoint of the beam defined in (11) in Table II.

The feedback force F_{fb} is generated by the voltage v_{e1} across R_{Q1}, given by

$$v_{e1} = -i_{z1}R_{Q1} \tag{25}$$

where i_{z1} is the resonator motional current indicated in Fig. 3, given by

$$i_{z1} = (v_{e1} - v_{b1})\frac{\partial C_1}{\partial z}\frac{\partial z}{\partial t}. \tag{26}$$

Inserting (26) into (25) and moving v_{e1} to one side yields

$$v_{e1} = \left[\frac{\frac{\partial C_1}{\partial z}\frac{\partial z}{\partial t}R_{Q1}}{1 + \frac{\partial C_1}{\partial z}\frac{\partial z}{\partial t}R_{Q1}}\right]v_{b1} \cong v_{b1}\frac{\partial C_1}{\partial z}\frac{\partial z}{\partial t}R_{Q1} \tag{27}$$

where the final form has been written with the assumption that the dc part of v_{b1} (i.e., V_{P1}) is much larger than any signal voltage v_{e1} arising on the input electrode. For this case,

$$\frac{\partial C_1}{\partial z}\frac{\partial z}{\partial t}R_{Q1} \approx \frac{v_{e1}}{V_{P1}}\frac{R_{Q1}}{R_{z1}} \ll 1 \tag{28}$$

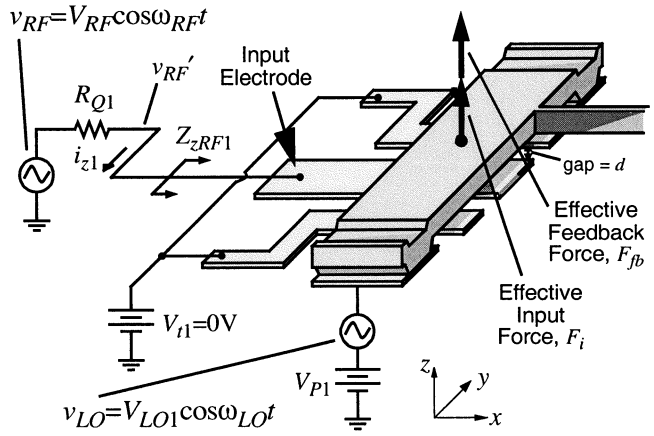

Fig. 3. Perspective-view schematic of a resistively loaded mixler input resonator defining force variables for Q-control and transfer function analyzes.

where R_{z1} is the series motional resistance of the resonator. For example, typical values for variables in (28) might be $(v_{e1}/V_{P1}) \approx 0.001$ and $(R_{Q1}/R_{z1}) \approx 10$, which result in a value of 0.01 for (28), much smaller than unity.

The expression for the feedback force F_{fb} can be found by inserting (27) into (1), assuming the input configuration of Fig. 3, then taking only terms at the vibration frequency $\omega_{\rm IF}$, since only these can counteract the input force term F_i. Doing so yields

$$\begin{aligned} F_{fb} &= -v_{b1}^1 \left(\frac{\partial C_1}{\partial z}\right)^2 \frac{\partial z}{\partial t} R_{Q1} \\ &= -\left(V_{P1}^2 + \frac{1}{2}V_{LO1}^2\right)\left(\frac{\partial C_1}{\partial z}\right) R_{Q1}(j\omega_{\rm IF} Z) \end{aligned} \quad (29)$$

where the final form is in phasor notation, with Z representing the phasor displacement. Inserting the phasor form of (29) into (24), then solving for Z, yields

$$Z = \frac{F_i Q'}{j k_{re}} \quad (30)$$

where Q' is the loaded (or controlled) quality factor, given by

$$Q' = Q\left(\frac{R'_{z1}}{R'_{z1} + R_{Q1}}\right) \quad (31)$$

and R'_z is an effective series motional resistance under mixing conditions, given by

$$R'_{z1} = \frac{k_{re}}{\omega_{\rm IF}\left(V_{P1}^2 + \frac{1}{2}V_{LO1}^2\right)\left(\frac{\partial C_1}{\partial z}\right)^2 Q}. \quad (32)$$

It should be noted that R'_{z1} is a quantity that is useful as shorthand in (31), but that is not the same as the series motional resistance R_{z1} of the input resonator.

Using (30)–(32), an expression for the termination resistance R_{Q1} for the input resonator to the mixler of Fig. 3 can now be written as [8]

$$\begin{aligned} R_{Q1} &= \left[\frac{Q}{q_1 Q_{\rm fltr}} - 1\right] R'_{z1} \\ &\approx \frac{k_{re}}{\omega_{\rm IF} q_1 Q_{\rm fltr}\left(V_{P1}^2 + \frac{1}{2}V_{LO1}^2\right)\left(\frac{\partial C_1}{\partial z}\right)^2} \end{aligned} \quad (33)$$

where q_1 is a normalized constant obtainable from filter cookbooks [16]. The main difference between (33) and the formula used for micromechanical filters is the addition of the (1/2) V_{LO1}^2 term, which can substantially lower the R_{Q1} required for a mixler over that for a nonmixing filter using the same mechanical network structure.

In the configuration of Fig. 1(b), since the local oscillator is only applied to the input resonator, and not to the output resonator, which receives only the dc-bias voltage V_{P2}, the Q-controlling termination resistor needed at the output port is the same as for a nonmixing filter, given by (9) in Table II. In the general case, however, where a local oscillator may also be applied to the output resonator, the expression for R_{Q2} takes on a form identical to that of (33), with 1 replaced by 2.

As for the case of μmechanical filters, (33) for mixlers stipulates that if small termination resistor values are desired (e.g., $R_{Qi} < 1$ kΩ), the electrode-to-resonator gap spacings of the constituent resonators should be made as small as permitted by dynamic range requirements [8], [17]. For this reason, the devices of this work utilize gap spacings on the order of 325 Å.

C. Mixler RF Input Impedance

For later determination of the transfer function for a mixler, the impedance $Z_{zRF1}(j\omega)$ seen at RF frequencies $\omega_{\rm RF}$ into the input port of the mixler is needed. $Z_{zRF1}(j\omega)$ can be derived by determining the input current at $\omega_{\rm RF}$ generated by an RF voltage $v'_{\rm RF} = V'_{\rm RF}\cos\omega_{\rm RF}t$ applied to the input port under the mixler excitation configuration shown in Fig. 1(b). (The prime notation distinguishes the input voltage $v_{\rm RF}$ from the actual voltage at the input electrode, which can be smaller due to loading.) For this derivation, we assume that $\omega_{\rm LO}$ is chosen such that the frequency difference $(\omega_{\rm RF} - \omega_{\rm LO})$ falls within the IF passband of the filter section of this device, for which case, a finite displacement z is induced. Under these conditions, the total current i_{zRF1} entering the input port *at RF* is given by

$$\begin{aligned} i_{zRF1} &= \left(C_{01} + \frac{\partial C_1}{\partial z} z\right)\frac{d}{dt}(v_{e1} - v_{b1}) \\ &\quad + (v_{e1} - v_{b1})\frac{\partial C_1}{\partial z}\frac{\partial z}{\partial t} \\ &= \cdots - z\frac{\partial C_1}{\partial z}\frac{\partial v_{LO1}}{\partial t} - v_{LO1}\frac{\partial C_1}{\partial z}\frac{\partial z}{\partial t} + \cdots \end{aligned} \quad (34)$$

where only terms at $\omega_{\rm RF}$ are presented in the final form. Assuming the force-to-displacement transfer function for the mixler input resonator takes the form

$$z = \frac{F_{mix}}{k_{re}}\Theta(j\omega) \quad (35)$$

where $\Theta(j\omega)$ models the frequency dependence of the force-to-displacement transfer function and is a function of the resonator Q and impedance, and of the overall mixler loading configuration. In general, $\Theta(j\omega)$ contains both magnitude and phase components, and is best obtained via simulation (e.g., using SPICE). However, for frequencies in the passband and for which the mixing force F_{mix} and the IF input current i_{zIF1} are in phase, $\Theta(j\omega) = q_1 Q_{\rm fltr}$ for a two-resonator mixler such as in Fig. 1(b).

Using (35) together with $v'_{RF1} = V'_{RF1}\cos\omega_{\rm RF}t$ and $v_{LO1} = V_{LO1}\cos\omega_{\rm LO}t$, (34) can be solved for the mixler RF input impedance magnitude $|Z_{zRF1}(j\omega)|$

$$|Z_{zRF1}(j\omega)| = \left|\frac{V'_{RF1}(j\omega)}{I_{zRF1}(j\omega)}\right| = \frac{4k_{re}}{\omega|\Theta(j\omega_{\rm IF})|V_{LO1}^2\left(\frac{\partial C_1}{\partial z}\right)^2} \quad (36)$$

where ω is an RF frequency, and $\omega_{\rm IF} = \omega_{\rm RF} - \omega_{\rm LO}$. As will be seen, the fact that $|Z_{zRF1}(j\omega)|$ is not infinite implies conversion loss in this mixer, which can degrade the noise figure of the overall device.

D. Mixler Voltage Transfer Function

Pursuant to determining the voltage transfer function for the mixler of Fig. 1(b), the output voltage for the device is first expressed as

$$v_{IF2} = i_{zIF2} R_{Q2} \tag{37}$$

where i_{zIF2} is the output current resulting from an oscillating output resonator (resonator 2) at an IF frequency, given by (5). Inserting (5) into (37), then converting to phasor form, yields

$$V_{IF2} = j\omega_{\rm IF} \frac{\partial C_2}{\partial z} V_{P2} R_{Q2} Z \tag{38}$$

where V_{IF2} and Z are the phasor output voltage and output displacement, respectively, at IF. Using (35) and an approximate form of (9) from Table II

$$R_{Q2} = \frac{k_{re}}{\omega_{\rm IF}(q_2 Q_{\rm fltr}) V_{P2}^2 \left(\frac{\partial C_2}{\partial z}\right)^2} \tag{39}$$

which holds when $R_{z2} \ll R_{Q2}$, (38) can be solved for the RF input-to-IF output transfer function for the mixler:

$$\frac{V_{IF2}}{V_{RF1}}(j\omega) = -\frac{1}{2}\frac{j\Theta(j\omega)}{q_2 Q_{\rm fltr}} \frac{V_{LO1}}{V_{P2}} \frac{\left(\frac{\partial C_1}{\partial z}\right)}{\left(\frac{\partial C_2}{\partial z}\right)} \times \left[\frac{Z_{zRF1}(j\omega)}{Z_{zRF1}(j\omega) + R_{Q1}}\right]. \tag{40}$$

Evidently, (40) contains numerous ratios that can be used to raise or lower the overall voltage gain of the mixler device, hence, adjust its noise figure.

E. Noise Figure

The SSB noise figure for this device derives from a combination of mixer conversion loss (or gain) $L_{\rm conv}|_{\rm dB}$ and filter insertion loss $L_{\rm fltr}|_{\rm dB}$, and thus, can be expressed as

$$F = L_{\rm conv|_{dB}} + L_{\rm fltr|_{dB}}\ [\rm dB] \tag{41}$$

where $L_{\rm conv}$ is given by the reciprocal of the conversion gain

$$L_{\rm conv} = \frac{1}{G_{\rm conv}} = \left[2 \times \left|\frac{V_{IF2}}{V_{RF1}}(j\omega_0)\right|\right]^{-1}. \tag{42}$$

The factor of "2" in the conversion gain expression in the far right of (42) accounts for the (1/2) factor recovered when removing the voltage division imposed by impedance matching during a through measurement. Under appropriately impedance-matched conditions and with resonator Qs greater than 1000, possible values might be $L_{\rm conv}|_{\rm dB} = 3$ dB (with $V_{LO1} = V_{P2}$ and $R_{zRF1} = R_{Q1}$) and $Lfltr|_{\rm dB} = 2$ dB, leading to $F = 5$ dB–very good calculated performance for a combined mixer and filter using passive components. However, although possible, attaining this value of noise figure requires near ideal input/output conditions, which are not always available. In particular, as will be seen in Section V, the specific input configuration used in this work precluded optimal impedance matching, and the available test equipment did not allow $V_{LO1} = V_{P2}$. As a result, measured noise figures in Section V are somewhat worse than 5 dB.

IV. Fabrication

Micromechanical mixlers were designed using the above procedure, then fabricated using a polysilicon surface-micromachining process that was similar in all respects to one used previously for HF micromechanical filters [8], except for an extra implant blocking mask to define high-resistance ($\sim$35 MΩ) coupling beams and for a much thinner sacrificial oxide to define electrode-to-resonator gap spacings of only 325 Å. Although seemingly minor changes from previous processes, the need for a nonconductive coupling beam and for such small gaps actually substantially complicates the annealing and release procedures, respectively, for these VHF devices.

A. Nonconductive Coupling Beam

As mentioned in Section II, in order to suppress LO-to-IF feedthrough, the mixler device of Fig. 1(b) features a nonconductive coupling beam that capacitively separates the input and output resonators. Note that if the source providing V_{P2} to the second resonator were ideal (with zero source resistance) and the series resistance in the second resonator were small, the LO signal feeding across the coupling beam capacitance would ideally be shunted to ac ground before reaching the IF port, effectively eliminating LO-to-IF coupling through the structure. In reality, finite resistivity in the resonator material allows some amount of LO-to-IF leakage, which can be suppressed by capacitively separating the input and output resonators.

To affect capacitive separation, the coupling beams of mixlers are merely made undoped by masking them during the resonator implant step of the fabrication process. The main drawback with this technique is that, due to a need to suppress dopant diffusion, which is much faster in polysilicon than single-crystal, the 1 hour anneal step at 1050 °C used in [8] can no longer be used to relieve stress and distribute implanted dopants. Instead, a carefully timed rapid-thermal anneal for 1.1 min at 1000 °C is used, yielding coupling beams with end-to-end resistances on the order of 35 MΩ.

B. 325 Å Electrode-to-Resonator Gaps

Because diffusion is difficult through small gaps for both reactants and etch byproducts [18], [19], release etch times for the 325 Å electrode-to-resonator gaps of this paper are much longer than for previous large-gapped surface micromachining processes. In particular, 25–45 min are required for 325 Å gaps in 48.8 wt.%HF, as opposed to $\sim$2 min. for 2 μm gaps. Due to a finite rate of attack by hydrofluoric acid (HF) on heavily doped polysilicon, longer release etch times often result in corrosion of polysilicon interconnect, with consequent resistivity increases, or even removal of interconnect entirely. Although metallization helps to reduce interconnect resistance, it cannot cover all interconnect areas, specifically, those areas within about a 4 μm spacing from the resonator structure. As a consequence, even with metallization present, interconnect resistances R_p up to 200 Ω are commonly seen for structures released using straight HF solutions, sans any of the additions to be described. Because R_zs can be as small as 20 Ω for devices with 325 Å electrode-to-resonator gaps and V_P's > 20 V, an $R_p \sim 200\ \Omega$ can seriously degrade a resonator's Q, in some cases by up to a factor of 10.

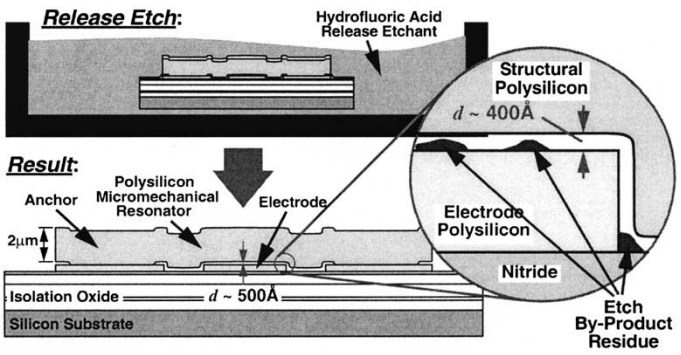

Fig. 4. Illustration depicting problems with etch byproduct residues when attempting to release a structure with a sub-500 Å electrode-to-resonator gap.

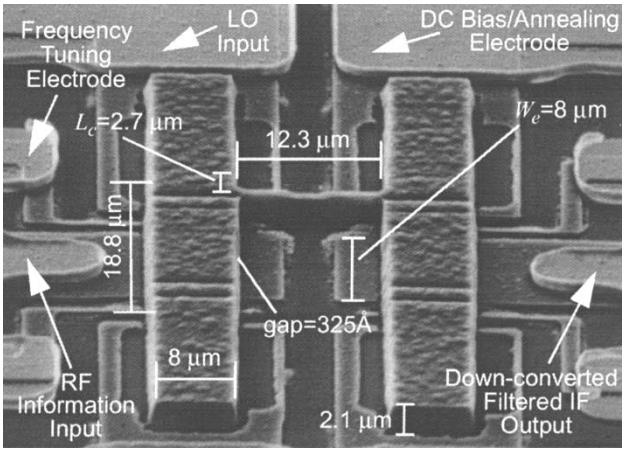

Fig. 5. Full-view SEM of a 37 MHz μmechanical mixler indicating key features and dimensions.

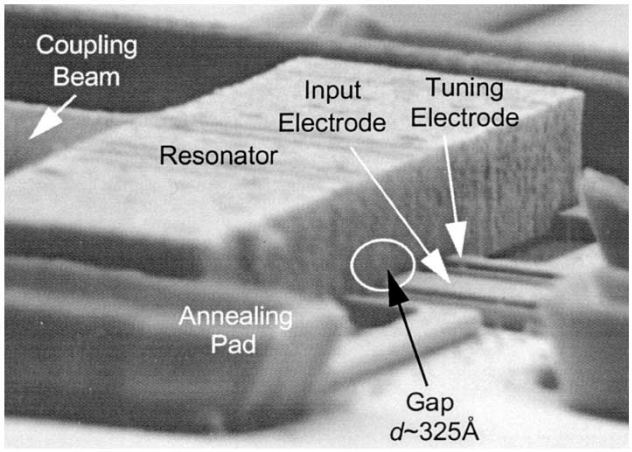

Fig. 6. Zoom-in side-view SEM showing vertical sidewalls and the tiny electrode-to-resonator gap.

Furthermore, and perhaps more importantly, there is some evidence that etch byproduct residues can actually remain in the tiny electrode-to-resonator gaps after release [20], [21], such as illustrated in Fig. 4. Such residues then behave as physical dampers during beam vibration and can severely degrade the Q of a given device. In severe cases (e.g., solid residues), resonator vibration might even be prevented entirely.

In an attempt to circumvent the above, the hydrocarbon-based surfactant, Triton X, was incorporated into some of the HF release etch solutions used for this work. The selection of Triton X to solve the present problem was motivated by its past use as a surfactant in buffered hydrofluoric acid (BHF) solutions in ULSI CMOS processes to improve yields when wet etching residual or native oxides in contact windows before metallization [22]. Briefly, Triton X enhances the ability of BHF to wet surfaces, and thus, to diffuse to the bottom of high-aspect-ratio contact windows and remove residual oxides. For the present purpose of removing oxide in tiny electrode-to-resonator gaps, the addition of Triton X to the HF release etch solution serves to (1) increase the ability of HF to wet surfaces, allowing it to more easily (and more quickly) diffuse into and etch away sacrificial oxide in the tiny gaps; (2) suppress the build-up of etch byproducts; and (3) reduce the adhesion of particulates on the beam surfaces. The use of surfactant-enriched HF also reduced the etch time required to release structures with 325 Å electrode-to-resonator gaps, from 45 min without the surfactant, to 25 min with it.

In addition to the above release-etchant modifications, extensive cleaning procedures were required immediately after release, involving repeated rinses in DI water, and sometimes even including an additional supercritical CO_2 cleaning step. The latter was not needed to prevent stiction of devices [23] (since the high stiffness of VHF devices very effectively prevents sticking), but rather to clean devices and purge contaminants from gaps.

V. Experimental Results

Several fabrication processes were run to achieve devices with varying electrode-to-resonator gaps from 300 Å to 1000 Å. Figs. 5 and 6 present wide- and zoomed-view scanning electron micrographs (SEMs) of a fabricated 37 MHz IF mixler device, indicating key dimensions and features. Table III summarizes the design of this mixler. In addition to mixler devices, process runs also included clamped-clamped beam μmechanical resonator devices at various VHF frequencies. These were included to extract design parameter values (e.g., Q, R_x, d) from the individual resonators making up the mixlers for purposes of verifying the analytical models of Sections II and III.

The use of the Triton X surfactant in the release solution was clearly beneficial to the yield rate of devices with electrode-to-resonator gaps smaller than 500 Å. In particular, without the use of surfactant-enriched HF in the release process, only about 25% of the mixlers with 325 Å-gaps on any given die were operable immediately after fabrication. The rest could not be operated without an additional postfabrication localized annealing step immediately before operation that burns away contaminants in the electrode-to-resonator gap and significantly raises the Q of devices, from about 500 to 2000 [20]. The use of surfactant-enriched HF in the release process increased the number of devices operable *without* annealing to about 75%. However, as described in [20], annealing was still required to attain Qs around 2000. In addition, it should be noted that "anneal-activation" was not required for devices with electrode-to-resonator gaps larger than 500 Å.

To minimize parasitic capacitance, mixlers, as well as stand-alone resonators, were attached and bonded directly to circuit

TABLE III
MIXLER DESIGN SUMMARY

Parameter	Value		Unit
	Design	Input/Sim.	
Resonator Beam Length, L_r	18.8	18.8	μm
Resonator Beam Width, W_r	8	8	μm
Physical PolySi Film Thickness, h	2.1	2.1*	μm
Eff. PolySi Film Thickness, h_{reff}	1.73	1.73†	μm
Coupling Location, L_c	2.7‡	**3.1**	μm
Coupling Beam Length, L_{s12}	12.3	12.3	μm
Coupling Beam Width, W_{s12}	1.5	1.5	μm
Coupling Beam Thickness, h_{s12}	2.1	2.1	μm
Electrode-to-Resonator Gap, d	325	325	Å
I/O Electrode Width, W_e	8	8	μm
Tuning Elec. 1 Edges: L_{t11}, L_{t12}	3, 4.4	3, 4.4	μm
Tuning Elec. 2 Edges: L_{t21}, L_{t22}	14.4, 15.8	14.4, 15.8	μm
Young's Modulus, E	150	150	GPa
Poisson Ratio, ν	0.226	0.226	—
Resonator Stiffness, $k_{re}(y=L_r/2)$	—	12,786	N/m
Resonator Mass, $m_{re}(y=L_r/2)$	—	0.237	ng
Coupling Beam Stiffness, k_{s12a}	—	2,598	N/m

* The physical thickness is used for coupling spring thickness in the simulation, but not for resonator thickness†.
† The effective thickness includes the effect of electrode-derived topography in resonators.
‡ Point coinciding with the center of the coupling beam width.

boards containing the needed electronics shown in Fig. 1(b), then evaluated inside a custom-built vacuum chamber under 50 μtorr pressure (provided by a turbo-molecular pump). Even at this low pressure, contaminants are still suspected in the system, perhaps due to outgassing from the board and electronics. An HP 8714C Network Analyzer was used with the above chamber and electronics to obtain frequency spectra for the stand-alone resonators and filters.

A. Resonator Q and Electrode-to-Resonator Gap Spacing

To obtain measured values for important mixler design parameters (e.g., Q, d_o, and $h_{\rm reff}$), frequency characteristics for stand-alone μmechanical resonators were obtained first. Fig. 7 presents the frequency characteristic for a 35.7 MHz, 325 Å-gapped μmechanical resonator, measured under 50 μtorr vacuum with $V_P = 11$ V and without annealing. Here, a Q of 550 is seen, which is smaller than actually achievable due to a lack of annealing. Note that unannealed resonators are characterized here, because localized annealing will not be possible for the mixlers to be tested next. This is because dopant diffusion in polysilicon is much faster than in single-crystal silicon, so even short anneals at the > 1000 °C temperatures produced seem to redistribute dopants in the mixler structure to the point of significantly lowering the resistance across the (supposedly nonconductive) coupling beam.

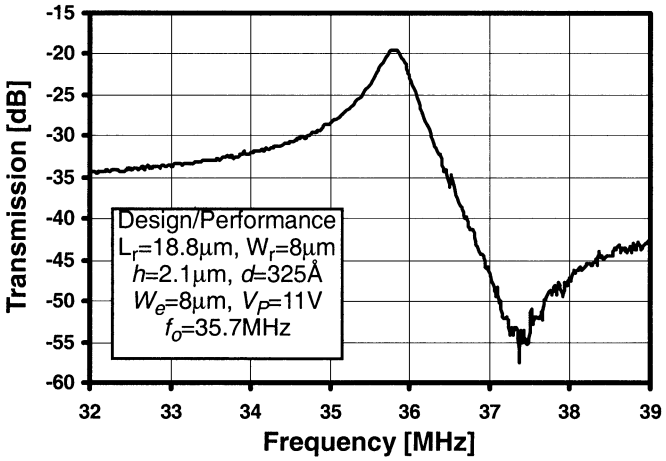

Fig. 7. Frequency characteristic for a 35.7 MHz μmechanical resonator measured under 50 μtorr vacuum with $V_P = 11$ V.

To determine the needed values of R_{Q1} and R_{Q2} for proper mixler operation, an accurate value of the electrode-to-resonator gap spacing d_o is required. However, as described in previous literature [8], [21], the electrode-to-resonator gap spacing d_o is often difficult to specify exactly. In particular, d_o is not specified solely by the sacrificial oxide thickness, but rather depends additionally on semiconductor depletion effects and the finite etch rate of polysilicon in HF during the release step, both of which can make the actual d_o significantly larger than the sacrificial oxide thickness.

Among the more effective methods for determining an accurate value for d in a given resonator is to first measure frequency as a function of dc-bias V_P, then match the measured curve to that predicted by (21) using d_o and the effective resonator thickness $h_{\rm reff}$, as fitting variables. This procedure not only determines an accurate value for the actual d_o, but also yields a value for $h_{\rm reff}$ that models the frequency-lowering effect of resonator topography [8]. Fig. 8 presents one such measured and matched curve for a $\sim$27 MHz micromechanical resonator fabricated alongside the mixlers in this paper. The matching procedure not only identifies the actual gap spacing and the effective thickness as 325 Å and 1.52 μm, respectively, for this resonator, but also, given the degree of matching, instills confidence in (21). In addition, the fact that the extracted effective thickness is more than 25% smaller than the actual thickness of the structural material underscores the importance of topography for VHF clamped-clamped beam micromechanical resonators.

B. Frequency Versus Local Oscillator Amplitude

To verify the dependence of resonance frequency on the local oscillator amplitude predicted by (21), Fig. 9 presents a plot of resonance frequency versus local oscillator amplitude $V_{\rm LO}$ for a 40.76-MHz μmechanical resonator subjected to the input configuration shown in Fig. 1(b), with $V_P = 17$ V. The theoretical prediction of (21) is also plotted, showing close agreement between theory and measurement, and showing an effective electrode-to-resonator gap spacing of 720 Å. (This resonator came

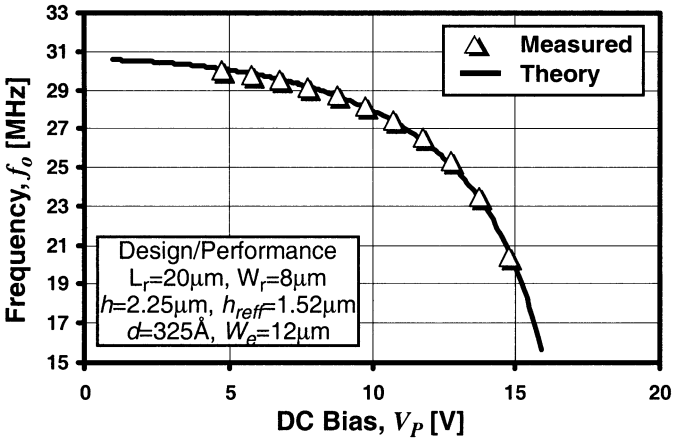

Fig. 8. Plots of measured and theoretical resonance frequency f_o versus dc-bias voltage V_P for a 20 μm-long, $\sim$27 MHz μmechanical resonator. The gap needed to match the theoretical curve to the measured one is 325 Å, and the effective thickness is 1.52 μm.

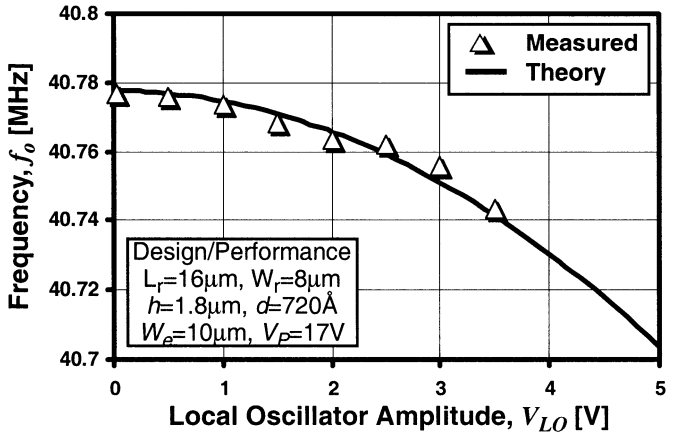

Fig. 9. Plots of measured and theoretical resonance frequency f_o versus local oscillator amplitude $V_{\rm LO}$ for a 40.76 MHz μmechanical resonator.

from a different run than did the mixlers of this paper, thus, the different gap spacing.)

C. Mixler Testing

The mixler device was first tested in IF filter mode, with $V_{\rm LO} = 0$ V, in order to verify that its filter function was operational. Using the fitted value of d_o determined earlier, and using the Q determined above, the values for R_{Q1} and R_{Q2} required to flatten the IF passband of the 37-MHz 630-kHz bandwidth μmechanical mixler structure were determined using (9) to both be 9.9 kΩ with $V_{P1} = V_{P2} = 11$ V and $V_{\rm LO} = 0$ V. For measurement, slightly smaller values for termination resistance of 5 kΩ each were used, in part to compensate for series resistance in the electrodes leading to the input and output resonators of the filter, and to alleviate problems with parasitic board capacitance.

Fig. 10 presents the measured IF filter response of the 37 MHz two-resonator mixler, showing 3.5 dB of insertion loss for a 1.7% bandwidth ($B = 630$ kHz), with a 20-dB down shape factor of 2.19. These values, along with other parameters defining the mixler's IF performance, are summarized in Table IV. It should be noted that, although adequate for IF applications, the performance of this filter does not convey the true

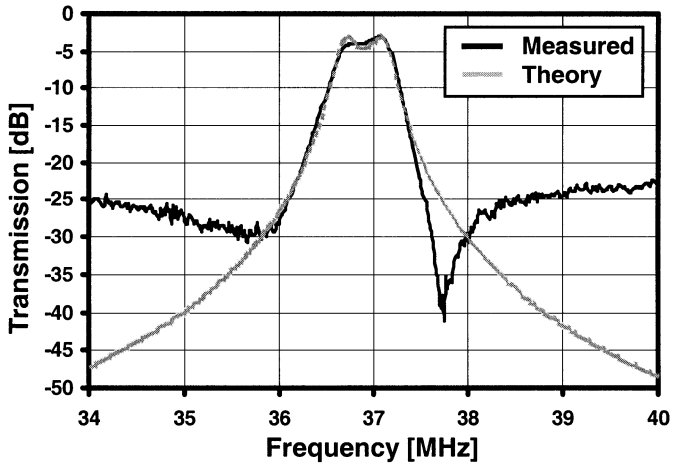

Fig. 10. Frequency characteristic for a 37 MHz micromechanical filter measured under 50 μtorr vacuum, along with the theoretical prediction. Data for both curves is included in Table III.

potential of this technology. In particular, a much smaller insertion loss should be achievable via a properly vacuum-encapsulated device, for which contamination is not an issue, allowing resonator Qs on the order of 2000 [20].

Mixler devices were then tested in full mixer-filter mode (i.e., with a nonzero $V_{\rm LO}$), using the setup shown in Fig. 11 and the inputs summarized in Table IV. Here, the output of a mixler device is monitored in the IF range (33–42 MHz) by a spectrum analyzer in MAX HOLD mode while the device is driven by an RF signal $v_{\rm RF}$ swept from 233–242 MHz, with a 200 MHz local oscillator voltage $v_{\rm LO}$ applied as in Fig. 1(b). In MAX HOLD mode, the spectrum analyzer retains the highest measured value seen at the frequency of the signal being measured. Under this measurement mode, by sweeping the input frequency over one range (e.g., the RF range), while measuring over another (e.g., the IF range), a spectrum analyzer can obtain a transmission spectrum over a frequency range different from the input frequency range. Although several sweeps are usually required to obtain sufficiently smooth spectra, this measurement approach can yield transmission spectra as good as attainable via a network analyzer, but without the network analyzer's constraint for identical input and output frequency ranges. Such a measurement set-up is obviously ideal for characterizing the subject mixler device.

It should be noted that the buffers in Fig. 11 are needed in this off-chip measurement system to reduce capacitive loading by coaxial lines, which when combined with the 5 $k\Omega$ R_{Qn}s used for the mixler under test, can introduce low frequency poles that reduce the 3-dB bandwidth of the measurement system to the point of denying measurement. These buffers would not be required in the fully integrated communication transceiver application targeted by these mixler devices, where transistor and micromechanical circuits are integrated onto single silicon chips [24]–[30], eliminating to a large extent the effects of capacitive loading. In the meantime, however, although the buffers do alleviate coax-derived losses, and hence make measurement possible, they do not eliminate finite bandwidth losses, since poles resulting from their input capacitance and the finite unity gain bandwidth of their op amps still contribute significant loss at 37

TABLE IV
MIXLER PERFORMANCE SUMMARY

Parameter	Value		Unit
	Measured	Simulated	
Local Oscillator Frequency, f_{LO}	200	200	MHz
P_{LO} Used in Measurement, P_{LOm}	15	15	dBm
V_{LO} Used in Measurement, V_{LOm}	3.56	3.56	V
V_P Used in Measurement, V_{Pm}	11	11	V
RF Frequency Range, f_{RF}	233-242	233-242	MHz
P_{RF} Used in Measurement, P_{RFm}	−10	−10	dBm
V_{RF} Used in Measurement, V_{RFm}	0.1	0.1	V
Freq. Tuning Voltage, V_{t1}	0†	0	V
Freq. Tuning Voltage, V_{t2}	8	8	V
Termination Resistor 1, R_{Q1}	5	**7**	kΩ
Termination Resistor 1, R_{Q2}	5	**7**	kΩ
Catastrophic Pull-In Voltage, V_{PI}	24 (meas.)	20.4	V
Resonator Quality Factor, Q	550	**500**	—
Resonator Series Resistance, R_z	8.67	3.15	kΩ
Filter Frequency, $f_o(V_P{=}V_{Pm})$	37.0	37.0	MHz
Filter Bandwidth, B	630	603‡	kHz
Filter Percent Bandwidth, (B/f_o)	1.70	1.63	%
Filter 20dB Shape Factor, S	2.19	2.5	—
Filter Insertion Loss, L_{fltr}	3.5	3.5	dB
Conv. Loss (f_{LO}=200MHz), L_{conv}	9.5†	9.46	dB
Combined Conv.-Ins. Loss, F	13†	12.96	dB
LO-to-IF Isolation (f_{LO}=200MHz)	39	—	dB
LO-to-RF Isolation (f_{LO}=200MHz)	29.4	—	dB
RF-to-IF Isolation (f_{RF}=237MHz)	44	—	dB

† The mixler was measured with the input resonator tuning and I/O electrodes combined to form the input port.
‡ Determined via a SPICE simulation using a filter equivalent circuit, such as in [8].

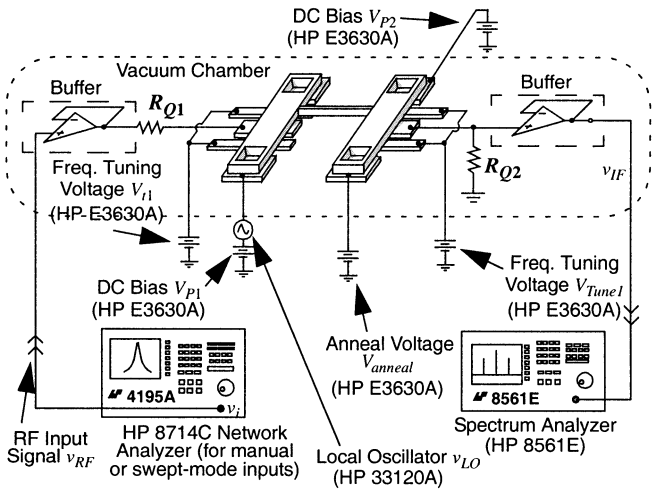

Fig. 11. Experimental set-up for mixler evaluation.

MHz. This loss will need to be subtracted out (i.e., baseline corrected) when determining the insertion loss of the mixler.

Using the above measurement strategy, the procedure for evaluating a 37 MHz mixler was as follows:

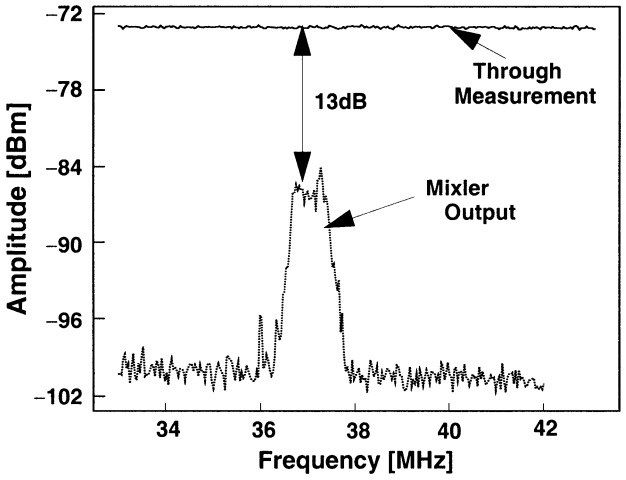

Fig. 12. Spectrum obtained when sweeping the RF input $v_{\rm RF}$ over a 233–242 MHz frequency range while detecting and holding outputs (using the MAX HOLD function on an HP 8561E Spectrum Analyzer) over a 33–42 MHz range.

1) With dc-biases $V_{P1} = V_{P2} = 11$ V, apply a 200 MHz local oscillator signal with $V_{\rm LO} = 3.56$ V as shown in Figs. 1(b) and 11, then measure a first spectrum by sweeping the RF input frequency from 233 to 242 MHz while monitoring the output from 33 to 42 MHz;
2) if the mixler passband is not flat, adjust the tuning voltages V_{tn} to move mode peaks so as to flatten/correct the filter passband; and
3) allow a sufficient number of sweeps to attain a smooth spectrum.

The result of this procedure is shown in Fig. 12, which shows the output spectrum of the mixler under RF excitation, as measured by a spectrum analyzer in MAX HOLD mode. Table IV summarizes other aspects of the input configuration used. It should be noted that, as indicated in Table IV, the particular mixler spectrum of Fig. 12 was measured with the I/O and tuning electrodes of the input resonator combined. By combining these electrodes, $(\partial C_1/\partial x)$ is made larger than $(\partial C_2/\partial x)$, so as to enhance the conversion gain of the mixing function, as predicted by (40). The fact that the IF filter spectrum is seen as the output under RF excitation clearly indicates downconversion and filtering.

A through measurement, in which the mixler device is bypassed by a short-circuit, is also included in Fig. 12, where losses from a combination of the low-frequency poles mentioned above and board parasitics are clearly seen. From the difference between this curve and the IF spectrum's peak signal, the total combined mixer conversion and filter insertion loss is 13 dB. Considering the 3.5 dB filter insertion loss measured in Fig. 10, the conversion loss is 9.5 dB, which is consistent with the prediction of (42) when using the stated V_P and $V_{\rm LO}$ values, and when accounting for the combined I/O-tuning electrode composition of the input resonator port. A more complete summary of the excitation signal levels used and performance obtained via this evaluation is included in Table IV.

D. Mixler Gain Versus Local Oscillator Amplitude

To further verify the accuracy of (40), the RF-to-IF gain of the 37-MHz mixler was measured as a function of local oscil-

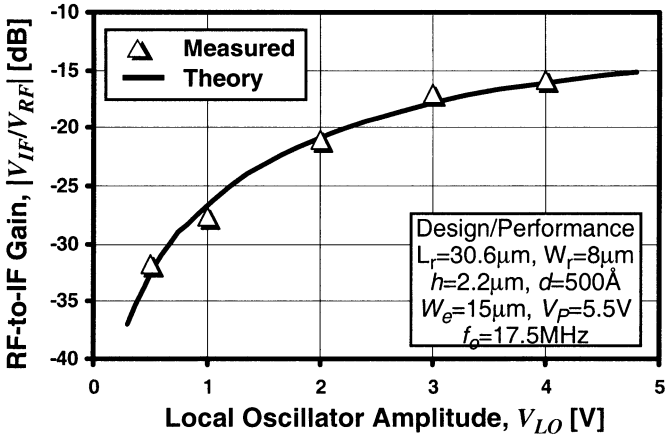

Fig. 13. Measured and predicted (using (40)) plots of combined conversion-insertion loss versus local oscillator amplitude.

lator amplitude $V_{\rm LO}$. The results for a 17.5-MHz version of the mixler are plotted in Fig. 13, alongside the theoretical prediction of (40), showing very good agreement between theory and measurement. Given the confidence that this and the previous result instill in (40), it is highly likely that the combined conversion-insertion loss of 5 dB predicted by (41) in Section III could be achieved if a signal generator capable of generating a local oscillator amplitude $V_{\rm LO}$ equal to $V_P = 11$ V were available.

E. Mixler Port-to-Port Isolation

In addition to the intended mixler parameters, the LO-to-IF, LO-to-RF, and RF-to-IF isolations were also measured for the mixler of Fig. 5. Results from these measurements are summarized in Table IV. It should be noted that, although already quite good, the data seen in Table IV most likely do not represent the true isolation capability of this technology, mainly because the device under test did not benefit from any planned shielding strategies. For example, if the device were fully integrated, and if the substrate were grounded instead of floating (as is the case for the devices of this work), then feedthrough currents associated with board and substrate parasitics would be eliminated, and the LO-to-IF and RF-to-IF path would pass through the mixler structure itself. Given the degree of feedthrough suppression afforded by dc-biasing the output resonator of the mixler, described in Section IV, the RF-to-IF and LO-to-IF isolations in this case should be substantially better, by several orders of magnitude.

VI. Measurement Versus Theory

In addition to designed and measured values, Tables III and IV, and Figs. 8–10 and 13, also include computed numbers and curves obtained via the analytical formulations of Sections II and III, and via SPICE simulations for the case of Fig. 10 using equivalent circuits similar to those presented in [8]. Tables III and IV list input or computed values under the "Input/Sim." and "Simulated" columns, respectively.

Only three major adjustments to the input data were required in order to match computed values to measured ones:

1) The coupling beam location L_c was changed from the design value of 2.7 μm to a computation input value of 3.1 μm in order to match the simulated bandwidth to the measured one. This is a reasonable modification given that the coupling beam actually has a finite width, so the actual coupling location is not necessarily at the point coinciding with the center of the coupling beam width, but could be elsewhere along this width.
2) The Q of the individual resonators used in the mixler was changed from the 550 measured on a 35.7–MHz resonator, to 500, in order to match the simulated insertion loss to the measured value. This is also quite reasonable, given that Q can easily vary by this amount from device to device.
3) The termination resistor values R_{Qn} for simulation were increased slightly above the actual experimental values to match the simulated filter passband ripple with that of the measurement. This too is reasonable, given that the series resistance in the I/O interconnect where metal is not present can be appreciable.

Each of these modifications is emphasized via boldface printing in Tables III and IV. With the above minor stipulations, the analytical formulations of Sections II and III are clearly quite accurate in predicting mixler performance. In particular, the new formulation for the integrated $(\partial C/\partial x)$ and the use of an effective thickness $h_{\rm eff}$ contribute positively to the degree of matching seen between theory and measurement. Given that the analytical formulation of this work predicts noise figures on the order of 5 dB in properly operated mixlers, such devices have great potential for use in paradigm-shifting MEMS-based transceiver architectures aimed at enhancing communication robustness and lowering RF power consumption [1].

VII. Conclusion

Micromechanical mixler devices have been demonstrated with IF frequencies in the low VHF range and SSB noise figures around 13 dB-performance on par with other mixer/filter combinations, both active and passive. Downconversion and filtering of RF signals from 200 MHz has been achieved. The need for large voltages, both ac magnitudes and dc bias levels, remains an issue for the mixlers of this work, but can be alleviated in future versions if smaller electrode-to-resonator gaps ($\sim$200 Å) are utilized. Alternatively, if larger impedances are allowed, which would be the case in fully integrated systems where both transistors and micromechanics are integrated together to reduce node capacitances, smaller gaps may not even be needed, and in fact larger gaps may be preferred for dynamic range reasons [17]. The verified analytical theory presented predicts that these approaches, coupled with more conductive interconnect, should actually allow mixler devices with substantially better noise figure than demonstrated here, which might then make possible paradigm-shifting MEMS-based transceiver architectures aimed at enhancing communication robustness and lowering RF power consumption [1].

References

[1] C. T. C. Nguyen, "Transceiver front-end architectures using vibrating micromechanical signal processors (invited)," in *Dig. Papers, Topical Meeting on Silicon Monolithic Integrated Circuits in RF Syst.*, Sept. 12–14, 2001, pp. 23–32.

[2] C. T.-C. Nguyen, "Frequency-selective MEMS for miniaturized low-power communication devices (invited)," *IEEE Trans. Microwave Theory Tech.*, vol. 47, pp. 1486–1503, Aug. 1999.

[3] M. L. Roukes, "Nanoelectromechanical systems," in *Tech. Digest, 2000 Solid-State Sensor and Actuator Workshop*, Hilton Head Island, SC, June 4–8, 2000, pp. 367–376.
[4] A.-C. Wong, H. Ding, and C. T.-C. Nguyen, "Micromechanical mixer + filters," in *Tech. Dig., IEEE Int. Electron Devices Meeting*, San Francisco, CA, Dec. 6–9, 1998, pp. 471–474.
[5] Maxim 2685 Data Sheet.
[6] Mini-Circuits JMS-1 Data Sheet.
[7] MuRata SAFCJ225MRA0X01 Data Sheet.
[8] F. D. Bannon III, J. R. Clark, and C. T.-C. Nguyen, "High frequency micromechanical filters," *IEEE J. Solid-State Circuits*, vol. 35, pp. 512–526, Apr. 2000.
[9] H. Nathanson, W. E. Newell, R. A. Wickstrom, and J. R. Davis Jr, "The resonant gate transistor," *IEEE Trans. Electron Devices*, vol. ED-4, pp. 117–133, Mar. 1967.
[10] H. A. C. Tilmans and R. Legtenberg, "Electrostatically driven vacuum-encapsulated polysilicon resonators: Part II. Theory and performance," *Sens. Actuators*, vol. A45, pp. 67–84, 1994.
[11] M. W. Putty, S. C. Chang, R. T. Howe, A. L. Robinson, and K. D. Wise, "One-port active polysilicon resonant microstructures," in *Proc. IEEE Micro Electro Mechanical Systems Workshop*, Salt Lake City, UT, Feb. 20–22, 1989, pp. 60–65.
[12] K. Wang, A.-C. Wong, W.-T. Hsu, and C. T.-C. Nguyen, "Frequency-trimming and Q-factor enhancement of micromechanical resonators via localized filament annealing," in *Dig. Tech. Papers, Transducers'97*, Chicago, IL, June 16–19, 1997, pp. 109–112.
[13] W.-T. Hsu, S. Lee, and C. T.-C. Nguyen, "In situ localized annealing for contamination resistance and enhanced stability in nickel micromechanical resonators," in *Dig. Tech. Papers, 10th Int. Conf. Solid-State Sensors and Actuators*, Sendai, Japan, June 7–10, 1999, pp. 932–935.
[14] W. Weaver Jr, S. P. Timoshenko, and D. H. Young, *Vibration Problems in Engineering*, 5th ed. New York: Wiley, 1990.
[15] W. Flugge, *Handbook of Engineering Mechanics*. New York: McGraw-Hill, 1962.
[16] A. I. Zverev, *Handbook of Filter Synthesis*. New York: John Wiley & Sons, 1967.
[17] R. Navid, J. R. Clark, M. Demirci, and C. T.-C. Ngyuen, "Third-order intermodulation distortion in capacitively-driven CC-beam micromechanical resonators," in *Tech. Dig., 14th Int. IEEE Micro Electro Mech. Syst. Conf.*, Interlaken, Switzerland, Jan. 21–25, 2001, pp. 228–231.
[18] D. J. Monk, D. S. Soane, and R. T. Howe, "Hydrofluoric acid etching of silicon dioxide sacrificial layers: I. Experimental observations," *J. Electrochem. Soc.*, vol. 141, no. 1, pp. 264–269, Jan. 1994.
[19] ——, "Hydrofluoric acid etching of silicon dioxide sacrificial layers: II. Modeling," *J. Electrochem. Soc.*, vol. 141, no. 1, pp. 270–274, Jan. 1994.
[20] A.-C. Wong, J. R. Clark, and C. T.-C. Nguyen, "Anneal-activated, tunable, 68 MHz micromechanical filters," in *Dig. Tech. Papers, 10th Int. Conf. Solid-State Sens. Actuators*, Sendai, Japan, June 7–10, 1999, pp. 1390–1393.
[21] K. Wang, A.-C. Wong, and C. T.-C. Nguyen, "VHF free-free beam high-Q micromechanical resonators," *J. Microelectromech. Syst.*, vol. 9, pp. 347–360, Sept. 2000.
[22] H. Kikyuama, N. Miki, K. Saka, J. Takano, I. Kawanabe, M. Miyashita, and T. Ohmi, "Principles of wet chemical processing in ULSI microfabrication," *IEEE Trans. Semicond. Manufact.*, vol. 4, pp. 26–35, Feb. 1991.
[23] G. T. Mulhern, D. S. Soane, and R. T. Howe, "Supercritical carbon dioxide drying of microstructures," in *7th Int. Conf. Solid-State Sens. Actuators (Transducers'93)*, Yokohama, Japan, June 1993, pp. 296–299.
[24] T. A. Core, W. K. Tsang, and S. J. Sherman, "Fabrication technology for an integrated surface-micromachined sensor," *Solid State Technol.*, pp. 39–47, Oct. 1993.
[25] J. H. Smith *et al.*, "Embedded micromechanical devices for the monolithic integration of MEMS with CMOS," in *Tech. Dig. IEEE Int. Electron Devices Meeting (IEDM)*, Wash., D.C, Dec. 10–13, 1995, pp. 609–612.
[26] J. M. Bustillo, G. K. Fedder, C. T.-C. Nguyen, and R. T. Howe, "Process technology for the modular integration of CMOS and polysilicon microstructures," *Microsyst. Technol.*, vol. 1, pp. 30–41, 1994.
[27] A. E. Franke, D. Bilic, D. T. Chang, P. T. Jones, T.-J. King, R. T. Howe, and G. C. Johnson, "Post-CMOS integration of germanium microstructures," in *Tech. Dig. 12th Int. IEEE MEMS Conf.*, Orlando, FL, Jan. 17–21, 1999, pp. 630–637.
[28] H. Baltes, O. Paul, and O. Brand, "Micromachined thermally based CMOS microsensors," *Proc. IEEE*, vol. 86, pp. 1660–1678, Aug. 1998.
[29] G. K. Fedder, S. Santhanam, M. L. Reed, S. C. Eagle, D. F. Guillou, M. S.-C. Lu, and L. R. Carley, "Laminated high-aspect-ratio microstructures in a conventional CMOS process," *Sens. Actuators*, vol. A57, no. 2, pp. 103–110, Mar. 1997.
[30] A.-C. Wong, Y. Xie, and C. T.-C. Nguyen, "A bonded-micro-platform technology for modular merging of RF MEMS and transistor circuits," in *Dig. Tech. Papers, 11th Int. Conf. Solid-State Sens. Actuators (Transducers'01)*, Munich, Germany, June 10–14, 2001, pp. 992–995.

Ark-Chew Wong (S'91–M'02) received the B.S. and M.S.E. degrees in electrical engineering from The Johns Hopkins University, Baltimore, MD, in 1994 and 1995, respectively, and the Ph.D. degree in electrical engineering and computer science from the University of Michigan, Ann Arbor, in 2001.

From 2001 to 2002, he was with the Transport Systems Solutions Division of Conexant Systems, Newport Beach, CA, where he designed analog and mixed-signal integrated circuits for SONET and gigabit ethernet applications. In 2003, he joined Globespanvirata, Irvine, CA, where he presently designs analog front ends for next-generation DSL.

Dr. Wong was the recipient of the Best Student Paper Award at the 1998 IEEE International Electron Devices Meeting. He is a member of Tau Beta Pi and Eta Kappa Nu.

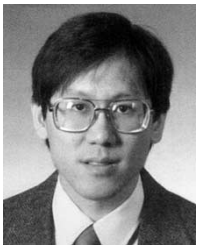

Clark T.-C. Nguyen (S'90–M'95–SM'01) received the B.S., M.S., and Ph.D. degrees from the University of California, Berkeley, in 1989, 1991, and 1994, respectively, all in Electrical engineering and computer sciences.

In 1995, he joined the University of Michigan, Ann Arbor, where he is presently an Associate Professor with the Department of Electrical Engineering and Computer Science. His research interests focus upon microelectromechanical systems and include integrated micromechanical signal processors and sensors, merged circuit/micromechanical technologies, RF communication architectures, and integrated circuit design and technology. From 1995 to 1997, he was a member of the National Aeronautics and Space Administration (NASA) New Millennium Integrated Product Development Team on Communications, which roadmapped future communications technologies for NASA use into the turn of the century. In 2001, he founded Discera, Inc., a company aimed at commercializing communication products based upon MEMS technology, with an initial focus on the very vibrating micromechanical resonators pioneered by his research in past years. He served as Vice President and Chief Technology Officer (CTO) of Discera until mid-2002, at which point he joined the Defense Advanced Research Projects Agency (DARPA) on an IPA, where he is presently the Program Manager of the MEMS, Micro Power Generation (MPG), Chip-Scale Atomic Clock (CSAC), MEMS Exchange (MX), Harsh Environment Robust Micromechanical Technology (HERMIT), Micro Gas Analyzers (MGA), and Radio Isotope Micropower Sources (RIMS) programs with the Microsystems Technology Office of DARPA.

Professor Nguyen received the 1938E Award for Research and Teaching Excellence from the University of Michigan in 1998, an EECS Departmental Achievement Award in 1999, the Ruth and Joel Spira Award for Teaching Excellence in 2000, and the University of Michigan's 2001 Henry Russel Award. Together with his students, he received the Roger A. Haken Best Student Paper Award at the 1998 IEEE International Electron Devices Meeting.